Processing and Application of Ceramics 6 [3] (2012) 123–131

Nanometric solid solutions of the fluorite and perovskite type crystal structures: Synthesis and properties

Snežana Bošković[1,*], Slavica Zec[1], Branko Matović[1], Zorana Dohčević-Mitrović[2], Zoran Popović[2], Matvei Zinkevich[3], Fritz Aldinger[3], Vladimir Krstić[4]

[1]*Institute of Nuclear Sciences "Vinča", University of Belgrade, POBox 522, 11001 Belgrade, Serbia*
[2]*Institute of Physics Belgrade, University of Belgrade, Pregrevica 118, 11080 Zemun, Serbia*
[3]*Max Planck Institute, Stuttgart, Heisenbergstr. 3, 70569 Stuttgart, Germany*
[4]*Queens University, Kingston, 45 Union Street, Ontario, Canada*

Received 20 December 2011; received in revised form 6 June 2012; accepted 10 July 2012

Abstract

In this paper a short review of our results on the synthesis of nanosized CeO_2, $CaMnO_3$ and $BaCeO_3$ solid solutions are presented. The nanopowders were prepared by two innovative methods: self propagating room temperature synthesis (SPRT) and modified glycine/nitrate procedure (MGNP). Different types of solid solutions with rare earth dopants in concentrations ranging from 0–0.25 mol% were synthesized. The reactions forming solid solutions were studied. In addition, the characteristics of prepared nanopowders, phenomena during sintering and the properties of sintered samples are discussed.

Keywords: *synthesis, nanopowders, fluorites, perovskites*

I. Introduction

Great attention has recently been paid to a development of a new generation of solid oxide fuel cells. The new generation of SOFC should be able to operate at much lower temperatures with rather high efficiency, as compared to currently developed ones. Therefore there is a demand for new materials which will fulfil the necessary conditions for the above said application. In addition, the materials should be less expensive, and produced by application of low cost technologies, including starting powders production. In order to be able to develop the compositions with high ionic conductivity which is needed for good electrolyte, many problems have to be solved starting with the powder synthesis [1,2].

The major objective of this paper is to present a short review of our results on highly effective and simple procedures [3–10] for synthesis of nanopowders that are good candidates for SOFC components. Since CeO_2 is known for its high ionic conductivity at lower temperatures, it is one of the most promising candidates to be used as an electrolyte. Many dopants, such as rare earth cations, show extended solid solubility in ceria lattice along with increasing ionic conductivity of CeO_2. On the other hand, doped Ce-manganites, as well as Ba-cerates, as a new generation of materials for future SOFC are also very attractive. We synthesized many different powders with perovskite type crystal structure (manganites and cerates) were produced, containing cation dopants on A as well as on B sites. Sintering tests were performed and these results are discussed, too. In addition, electrical properties for some of the sintered compositions are presented.

II. Experimental

2.1. SPRT - method

Self propagating room temperature synthesis (SPRT), used for preparation of different solid solutions ($CeO_{2-\delta}$, $Ce_{0.90}Y_{0.10}O_{2-\delta}$, $Ce_{0.85}Y_{0.15}O_{2-\delta}$, $Ce_{0.80}Y_{0.20}O_{2-\delta}$, $Ce_{0.75}Y_{0.25}O_{2-\delta}$, $Ce_{0.90}Nd_{0.10}O_{2-\delta}$, $Ce_{0.85}Nd_{0.15}O_{2-\delta}$, $Ce_{0.80}Nd_{0.20}O_{2-\delta}$, $Ce_{0.75}Nd_{0.25}O_{2-\delta}$ and $Ce_{0.80}Y_{0.10}Nd_{0.10}O_{2-\delta}$) was described in detail in our previous paper [3]. Starting reactants used in the experiments were cerium nitrate (Merck), yttrium nitrate (Alfa Aesar), neodymium nitrate (John Mathey) and sodium hydroxide. All used nitrates were

* Corresponding author: tel: +381 11 340 8480
fax: +381 11 340 8224, e-mail: boskovic@vinca.rs

in the form of hexahydrates. Amounts of nitrates and NaOH were calculated according to the nominal composition of the solid solutions. The chemicals were not milled. Hand-mixing was performed [3] in alumina mortar for 5–7 min until the mixture got light brown. After being exposed to air for 3 h, the mixture was suspended in water. Rinsing of $NaNO_3$ was performed in centrifuge - Megafuge 1.0, Heraeus, at 3200 rpm, for 10 min. This procedure was performed three times with distilled water and twice with ethanol.

2.2 MGNP-method

Modified glycine/nitrate procedure (MGNP), used for preparation of different solid solutions ($CaMnO_3$,$Ca_{0.7}La_{0.3}MnO_3$,$Ca_{0.9}Y_{0.1}MnO_3$,$Ca_{0.8}Y_{0.2}MnO_3$, $Ca_{0.7}Y_{0.3}MnO_3$,$Ca_{0.7}La_{0.3}Mn_{0.8}Ce_{0.2}O_3$,$BaCeO_3$,$BaCe_{0.9}Gd_{0.1}O_3$, $BaCe_{0.85}Gd_{0.15}O_3$, $BaCe_{0.8}Gd_{0.2}O_3$, $BaCe_{0.8}Nd_{0.2}O_3$ and $BaCe_{0.8}Sm_{0.2}O_3$) was described in detail in our previous paper [4]. Starting chemicals used for the synthesis of the powders were aminoaceteic acid-glycine, (Fischer Scientific, USA), metallic acetates (Mn, Ba) and nitrates (Ce, La, Y, Nd, Gd, Sm), produced by Aldrich, USA. All nitrate solutions were previously prepared and the cation concentration (in mg/ml) was determined by gravimetry. On the basis of these data, the portions of prepared solutions were taken according to previously calculated composition of the final powder. Synthesis was carried out in a stainless steel reactor in which all reactants dissolved in distilled water were added according to previously calculated composition of the final powder. We used nitrates in the form of solutions, and acetates in the as received form [4,5]. Glycine was also added in the as received form. The reactants were heated on a hot plate up to about 540 °C, until the evolution of the smoke terminated. As a result of modifying glycine/nitrate process (GNP), the reaction proceeded very smoothly. Therefore almost no loss in the synthesized powders quantity was observed. The experimentally obtained amount of powder was very close to the theoretically calculated one, 96–99%. For practical reasons it is very important to outline that the quantity of chemicals was designed to synthesise 100 g of powder per run (in 30 min), which is according to our knowledge among the largest scale produced by this method so far. Since the evaporation was not intense during the experiment, the amount of powder produced per run can be even larger if the size of reactor would increase. The obtained ashes were afterwards calcined depending on the composition, at temperatures 800–1050 °C, for 2–4 hours.

2.3 Processing of bulk ceramics

The synthesized powders were ball milled in ethanol with zirconia grinding media for 24 h and mean particle size was determined by "Horiba" laser particle size analyzer, using ethanol as dispersing fluid. Powders granulated with 5 wt.% of polyethylene glycol as a binder, were compacted by uniaxial pressing under 50 MPa and thereafter cold isostatic pressing under 200 MPa was applied. The burn out of the binder was accomplished under vacuum at 450 °C. Sintering was performed in the air in the temperature interval between 1100 °C to 1550 °C for 2 h at a heating rate of 4 °C/min up to 1000 °C and 2 °C/min up to sintering temperature.

2.4 Characterization

The dried and calcined powders were analysed by applying X-ray diffraction (XRD, Siemens D-5000), scanning electron microscopy (SEM, Zeiss DSM 982 Gemini), Raman spectroscopy (Jobin-Ivon monochromator) and specific surface area measurement (BET). Lattice parameters and crystallite size were obtained using PowderCell 2.4 program. Chemical analysis of dopants concentration was carried out by EDTA titration to check the difference between the nominal and true compositions of solid solution powders. To follow the reaction path, differential thermal analysis (DTA) and thermogravimetry (TG, Netzsch STA 409) were performed in air atmosphere, at heating and cooling rates of 5 °C/min.

Sintered densities were measured by Archimedes method in hexane. Electrical dc-resistance was measured by the four-point method in the range from 25 to 900 °C using "Agilent" multimeter. Resistance value vs. temperature was monitored after stabilisation.

III. Results and discussion

3.1 SPRT - reaction development

SPRT procedure is based on the self-propagating room temperature reaction [3] between metal nitrates and sodium hydroxide, and in the case of the doped ceria solid solution the reaction can be written as follows:

$$2[(1\text{-}x)Ce(NO_3)_3\cdot 6H_2O + xMe(NO_3)_3\cdot 6H_2O] + 6NaOH + (½\text{-}\delta)\,O_2 \rightarrow 2Ce_{1-x}Me_xO_{2-\delta} + 6NaNO_3 + 15H_2O$$

During heating of the reacting mixture of cerium nitrate, yttrium nitrate and NaOH weight loss started at 50°C as can be seen on TG curve (Fig. 1). Simultaneously with the observed effect, the rate of weight loss starts to increase (DTG curve) followed by endothermic effect, as found earlier [3]. The maximum reaction rate at 160 °C (Fig. 1) coincides with the termination of the heat release [3]. This indicates that the reaction is initiated by the rapid, strong heat release, developing easily afterwards.

However, from Fig. 2 it is clear that reaction is taking place via three intermediate steps, as DTG curve shows three peaks, which means that each endothermic effect is accompanied by definite mass loss connected with the loss of chemically bound water molecules from nitrates [3]. Weight loss terminates at 300 °C, at

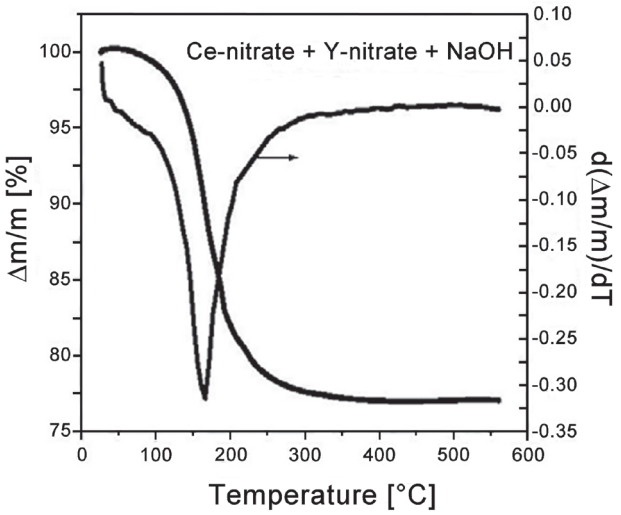

Figure 1. TG and DTG curves for homogenized cerium nitrate, yttrium nitrate and NaOH mixture

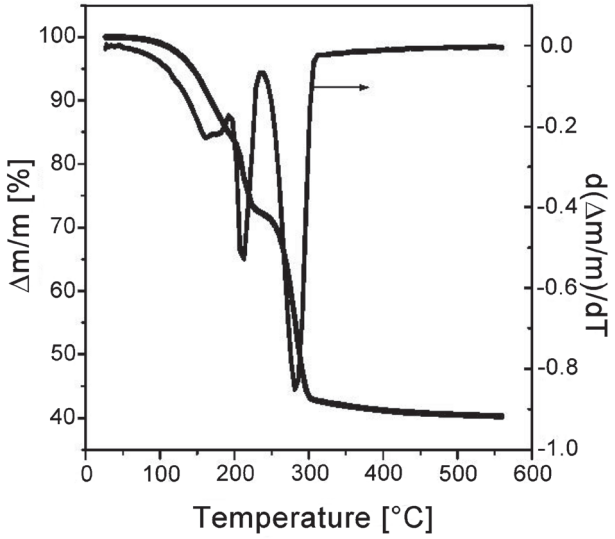

Figure 2. TG and DTG curves for pure $Ce(NO_3)_3 \cdot 6H_2O$

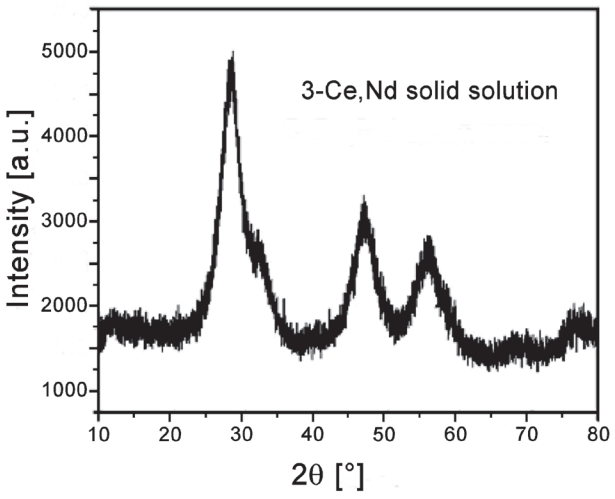

Figure 3. X-ray pattern of $Ce_{0.90}Nd_{0.10}O_{2-\delta}$ powder

this point cerium nitrate hexahydrate was completely converted into ceria after a gradual loss of crystalline water (Fig. 2). Extremely low reaction temperatures indicated that by introducing mechanic energy into the system, reaction would, also be easily initiated also. That is why hand mixing was performed.

XRD of final reaction product if cerium nitrate, neodymium nitrate and NaOH were mixed together is given in Fig. 3 [1,4,5]. This pattern revealed the characteristic peaks of $Ce_{0.90}Nd_{0.10}O_{2-\delta}$. The previously mentioned reaction steps, however, could be observed only with the non-homogenised mixture in which the reaction proceeds at much lower rate compared to homogenized mixture (Fig. 4). To make the reaction steps to be obvious, two substances $Ce(NO_3)_3 \cdot 6H_2O$ and NaOH, were brought into contact and just allowed to react for 24 h. In the X-ray pattern of this sample (Fig. 4), the diffraction lines of final reaction products CeO_2 and $NaNO_3$ were detected, along with intermediate reaction products that are mainly Ce-nitrates with lower number of crystalline water molecules. These results are in agreement with the ones in Fig. 2.

Raman spectroscopy was performed at room temperature to prove the formation of solid solutions. In Fig. 5 Raman spectra of pure CeO_2 and solid solution powders are presented. The solid solutions retain cerium fluorite structure without the Raman modes of pure dopant oxides. The shift to lower energies of the main F_{2g} Raman mode from 465 cm^{-1} (in bulk) to 454 cm^{-1} (CeO_2 sample) and its asymmetrical broadening indicate the strong phonon confinement effect in these nanopowders. In doped samples this mode is red or blue shifted regarding the CeO_2 nanostructured sample, depending on the dopant ionic size. Additional Raman mode at 599 cm^{-1} in pure ceria nanopowder [6–8] originates from intrinsic oxygen vacancies due to the powder's nonstoichiometry while the appearance of a new Raman feature in doped samples at 454 cm^{-1} is due to the extrinsic O^{2-} vacancies in fluorite structure in order to keep charge neutrality when Ce^{4+} ions are partly replaced with Nd^{3+}(Y^{3+}) ions. From the Raman spectra it can be concluded that we are not dealing with simple mechanical mixtures of oxides, but with their solid solutions. In addition to Raman spectroscopy results, lattice parameters dependence on dopants concentration was obtained and found to obey Vegard′s law, proving that solid solution were synthesized indeed [3].

Specific surface areas, crystallite size, particle size, true composition and sodium content after washing of the synthesized powders are given in Table 1 [3]. Crystallite size was obtained on the basis of XRD data, while the particle size was measured from SEM images (Fig. 6).

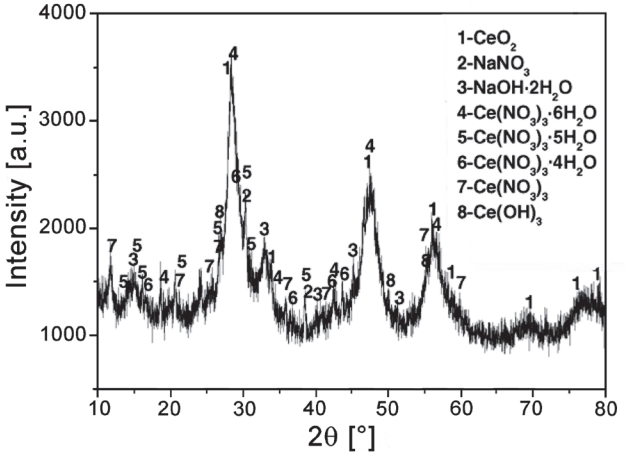

Figure 4. X-ray pattern of non-homogenized mixture

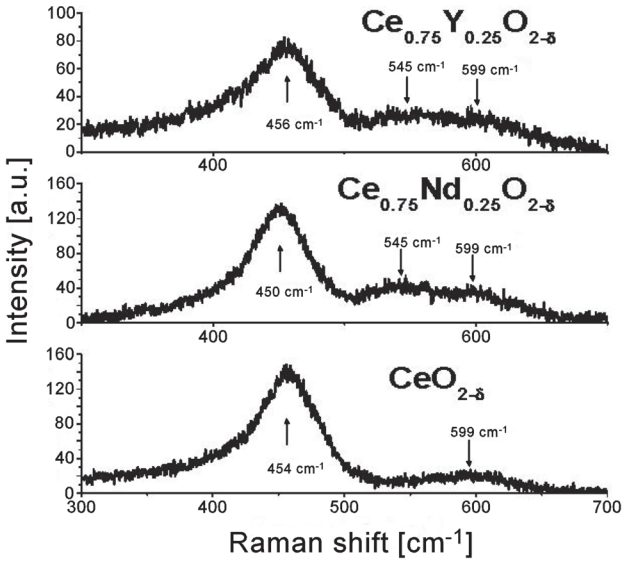

Figure 5. Raman spectra of pure and doped ceria

3.2 MGNP - procedure

Glycine-nitrate process is based on the self-combustion of the glycine and nitrate mixture ($Me^1(NO_3)_3 \cdot 6H_2O$ and $Me^2(NO_3)_3 \cdot 6H_2O$), according to the reaction that could be described with the following equation [4]:

$$2\ NH_2CH_2COOH + [Me^1(NO_3)_3 \cdot 6H_2O + Me^2(NO_3)_3 \cdot 6H_2O] + 2\ O_2 \rightarrow Me^1Me^2O_2 + 22\ H_2O\uparrow + 4\ N_2\uparrow + 4\ CO_2\uparrow$$

which spontaneously occurs at about 180°C. Glycine plays in this reaction double role, it acts as a fuel and on the other hand as a complexant. By complexing with present cations (Me^{1+4} and Me^{2+3}) their selective precipitation prior to ignition (after the water had been evaporated) is prevented. The reaction is, as mentioned, very intense and needs to be controlled. There are different possibilities to control the reaction rate, and thereby the reaction temperature in order to obtain finer particles and larger specific surface area.

We modified [4,9,10] the original GNP procedure [2] by replacing partially as discussed above, nitrates by acetates. Acetates are water soluble, and are less expensive compared to nitrates of the same purity. To prove the difference between powders obtained by GNP and MGNP we synthesized $CaMnO_3$ by both procedures. X-ray patterns of the two ashes [4] showed as the only difference the fact that $CaMnO_3$ ash obtained by GNP was better crystallised. This is due to higher temperatures developed during GNP as compared to MGNP. However, better crystallised powder due to faster growth of crystallites resulted in decreasing of specific surface area. By applying MGNP method we managed to produce different powders with more than one dopant cation, of very precise stoichiometry and with nanometric particle size. Most of the ashes that are obtained immediately after synthesis were partially amorphous. How-

Table 1. Properties and chemical analysis of as-prepared SPRT powders [3]

Composition	Crystallite size [nm]	Surface area [m^2/g]	Particle size [nm]	True composition	Na-content [wt.%]
CeO_2	4.18	106.9	16		
$Ce_{0.90}Y_{0.10}O_{2-\delta}$	4.25	103.2	14	$Ce_{0.904}Y_{0.096}O_{2-\delta}$	0.05
$Ce_{0.85}Y_{0.15}O_{2-\delta}$	4.22	137.1			
$Ce_{0.80}Y_{0.20}O_{2-\delta}$	4.99	109.7			
$Ce_{0.75}Y_{0.25}O_{2-\delta}$	5.62	94.0			
$Ce_{0.90}Nd_{0.10}O_{2-\delta}$	4.36	118.4		$Ce_{0.914}Nd_{0.086}O_{2-\delta}$	0.07
$Ce_{0.85}Nd_{0.15}O_{2-\delta}$	4.35	137.6			
$Ce_{0.80}Nd_{0.20}O_{2-\delta}$	4.19	141.5	10		
$Ce_{0.75}Nd_{0.25}O_{2-\delta}$	4.12	99.6		$Ce_{0.78}Nd_{0.22}O_{2-\delta}$	0.005*
$Ce_{0.80}Y_{0.10}Nd_{0.10}O_{2-\delta}$	4.49	110.0	12	$Ce_{0.828}Y_{0.085}Nd_{0.087}O_{2-\delta}$	0.008*

*increased number of rinsing runs

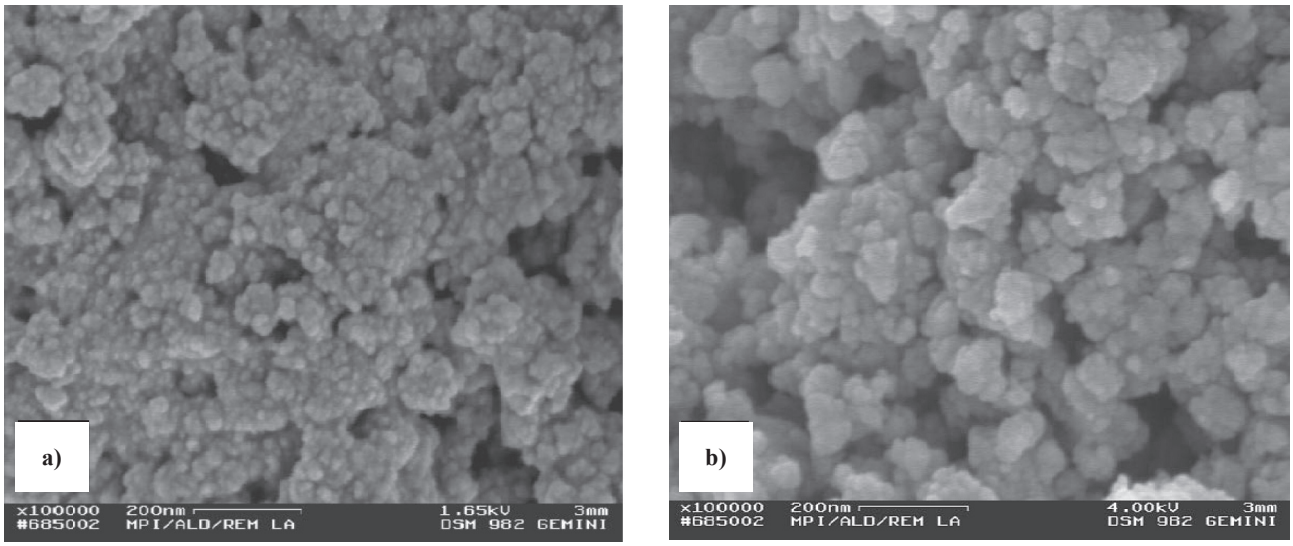

Figure 6. Y doped (a) and Y, Nd co-doped (b) ceria solid solutions

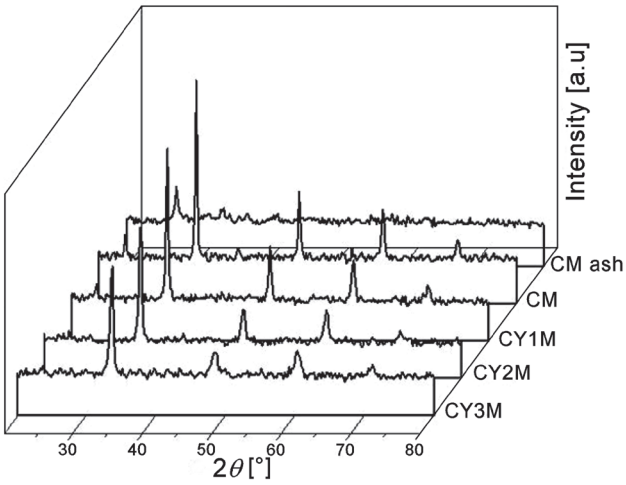

Figure 7. X-ray patterns of $CaMnO_3$ compositions

ever, the powders obtained after calcination were all single- phase powders, i.e. solid solutions. Peaks related to isolated dopant oxides or secondary phases were not observed. All of them exhibit perovskite type crystal structure. The example in Fig. 7 is given for Y-doped $CaMnO_3$. The XRD patterns of all powders look

similar to each other, despite the different amount of dopant. However, a slight difference of peak widths as well as the shifting of the peaks toward lower angles with increasing dopant amounts can be observed. This indicated the existence of solid solution (Fig. 7). Microstructure size-strain analysis showed both crystallite size and crystallite strain increase with dopant insertion into perovskite structure. In cerate group of powders (calcined at 1050 °C for 4 h) specific surface area almost does not change neither with cation type nor with the dopants con-

Table 2. Specific surface area and dopants concentrations for MGNP powders [4,5]

No	Nominal composition $A_{1-x}B_xO_3$	Surface area [m^2/g]	Dopants content [wt.%]	***x*** in $A_{1-x}B_xO_3$
1	$CaMnO_3$	17.7	-	-
2	$Ca_{0.7}La_{0.3}MnO_3$	9.9	19.5±0.4	0.245
3	$Ca_{0.9}Y_{0.1}MnO_3$	17.5	6.13±0.12	0.102
4	$Ca_{0.8}Y_{0.2}MnO_3$	16.3	11.3±0.2	0.195
5	$Ca_{0.7}Y_{0.3}MnO_3$	15.6	16.2±0.3	0.288
6	$Ca_{0.7}La_{0.3}Ce_{0.2}Mn_{0.8}O_3$	13.2	20.8±0.4 (La) 13.5±0.3 (Ce)	0.289
7	$BaCeO_3$	3.6	-	-
8	$BaCe_{0.9}Gd_{0.1}O_3$	3.4	4.46±0.06	0.093
9	$BaCe_{0.85}Gd_{0.15}O_3$	3.1	6.51±0.09	0.164
10	$BaCe_{0.8}Gd_{0.2}O_3$	3.5	7.79±0.12	0.180
11	$BaCe_{0.8}Nd_{0.2}O_3$	3.6	7.82±0.12	0.177
12	$BaCe_{0.8}Sm_{0.2}O_3$	3.5	8.86±0.14	0.193

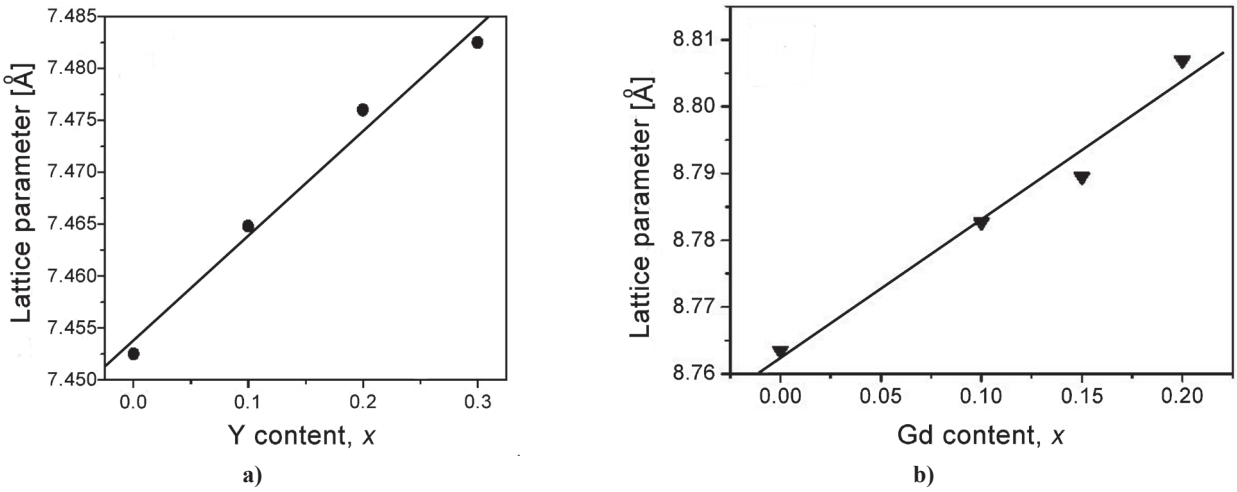

Figure 8. Lattice parameters of (a) $Ca_{1-x}Y_xMnO_3$ and (b) $BaCe_{1-x}Gd_xO_3$ as a function of Y and Gd contents, respectively

centration, although the concentration of dopants was doubled (the samples 8 and 10, Table 2). It seems that with increasing calcination temperature specific surface area decreases drastically, and all other factors influencing specific surface area are masked. Chemical analysis data (Table 2) show excellent agreement between designed and true composition of all synthesized powders.

Lattice parameters were calculated for all the calcined powders. The results are presented in Fig. 8 as the dependence of lattice parameters on dopants concentration (x), as well as, in Fig. 9 as the dependence of lattice parameters on the dopants cation radii (Ba^{2+} - 1.34 Å, Ce^{4+} - 0.920 Å, Gd^{3+} - 0.938 Å, Sm^{3+} - 0.964 Å, Nd^{3+} - 0.995 Å) [11]. In $CaMnO_3$ doped with Y^{3+}, lattice parameters obey Vegard's law as shown in Fig. 8. The same was found for lattice parameter dependence on Gd concentration in Ba-cerates. Data in Figs. 8 and 9 are very important since phase diagrams are not always known, for they prove, too, that single phase powders were obtained in the investigated concentration range. SEM and TEM analyses were performed for manganites and cerates, respectively.

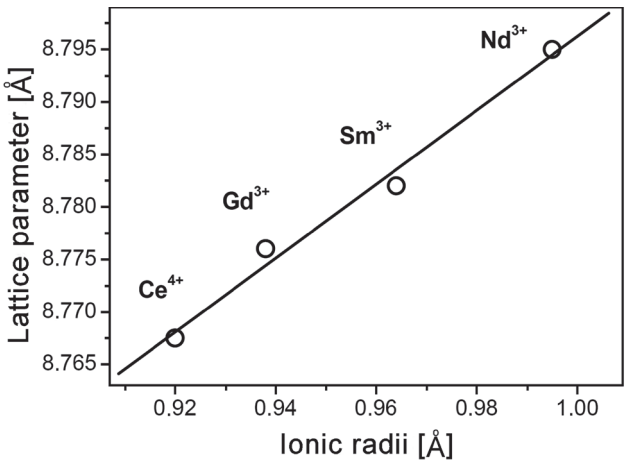

Figure 9. Lattice parameters of $BaCeO_3$ as a function of ionic radii of dopants (Ce^{4+}, Gd^{3+}, Sm^{3+}, Nd^{3+})

Ca-manganite particles were less than 50 nm in size, which is illustrated in TEM image presented in Fig. 10 for $Ca_{0.8}Y_{0.2}MnO_3$ powders obtained after calcining at 800 °C for 4 h. Insert picture in the upper right side shows the typical electron diffraction image of the nanocrystal surface which appears disordered, or even amorphous. This matches the XRD results, where short-range order of nanoparticles exhibits diffraction patterns with pronounced X-ray peak broadening [9,10]. On the other hand, the size of particles of $BaCe_{0.9}Gd_{0.1}O_3$ after calcinations at 1050 °C for 4 h lies in the range of 80–100 nm. It is also obvious from Fig. 10, that cerate particles have already been sintered during calcination, which is in accordance with the results obtained for the specific surface area (Table 2), contrary to managanites particles that are calcined as mentioned, at much lower temperature.

3.3 Sintering of calcium manganite powders

Green densities of the compositions studied are given in Table 3 [7]. Optimum sintering temperatures were determined experimentally for each composition in the range from 1000–1550 °C. Optimum sintering temperature was considered the one at which highest density was achieved and these data together with sintered densities and the difference between sintered and green densities [7] are summarized in Table 4.

Since specific surface areas and particle size do not differ too much, sintered density values indicate that increasing Y concentration enhanced densification of Ca-manganite [7]. The density data obtained at 1150 °C for all the Y containing solid solutions show clearly that sintered density increases with increasing Y content in the solid solution. However, the La addition affects the increase of the sintering temperature of Ca-manganite, especially in the presence of Ce ions whereby the densification degree dropped. In spite of relatively high specific surface area of these samples, sintering temperature turns to be the highest. The in-

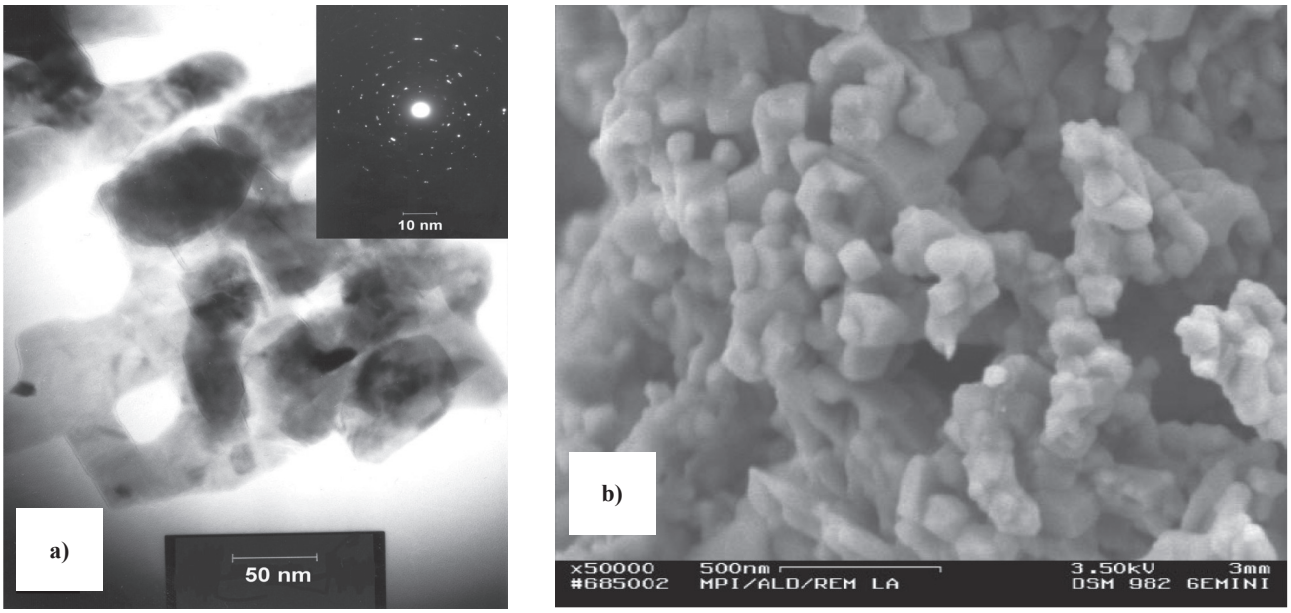

Figure 10. Microstructures of (a) $Ca_{0.8}Y_{0.2}MnO_3$ (TEM) and (b) $BaCe_{0.9}Gd_{0.1}O_3$ (SEM) powders

fluence of dopants concentration on the densification during sintering can be discussed only in the case of Y containing samples. Namely, with increasing Y^{3+} ions in the lattice of $CaMnO_3$ on A site, cation vacancies are created [7,9]. For two Y^{3+} ions introduced into the lattice on A site instead of Ca^{2+}, one cation vacancy is formed for charge compensation. Increasing cation vacancy concentration is not relevant for the increased densification degree, since the rate determining step is oxygen diffusion. However, bearing in mind the

Table 3. Green densities of selected compositions [7]

Designation	Composition	Green density [g/cm^3]	TD [%]
CM	$CaMnO_3$	2.2	47.2
CY1M	$Ca_{0.9}Y_{0.1}MnO_3$	1.9	40.9
CY2M	$Ca_{0.8}Y_{0.2}MnO_3$	1.9	39.7
CY3M	$Ca_{0.7}Y_{0.3}MnO_3$	2.0	39.1
CLM	$Ca_{0.7}La_{0.3}MnO_3$	2.4	42.6
CLMC	$Ca_{0.7}La_{0.3}Mn_{0.8}Ce_{0.2}O_3$	2.2	35.9

Table 4. Sintering temperatures, sintered densities and d_s-d_i parameter [7]

Designation	Nominal composition	Sintering temperature [ºC]	Sintered density [g/cm^3]	Sintered density [TD %]	d_s-d_i** [%]
CM	$CaMnO_3$	1250*	4.54	99.1	-
CM	$CaMnO_3$	1150	4.06	88.6	51.6
CY1M	$Ca_{0.9}Y_{0.1}MnO_3$	1200*	4.48	94.9	-
CY1M	$Ca_{0.9}Y_{0.1}MnO_3$	1150	4.38	92.8	-
CY2M	$Ca_{0.8}Y_{0.2}MnO_3$	1150*	4.40	91.0	51.3
CY3M	$Ca_{0.7}Y_{0.3}MnO_3$	1150*	4.84	94.5	53.1
CLM	$Ca_{0.7}La_{0.3}MnO_3$	1350*	5.20	94.2	55.4
CLMC	$Ca_{0.7}La_{0.3}Mn_{0.8}Ce_{0.2}O_3$	1450*	5.29	87.4	-

*Optimum sintering temperature
** d_s-sintered density, d_i-green density (TD%)

case when cation vacancies are dominant lattice defects in the bulk, the grain boundary charge is expected to be positive [12] and would be responsible for enhanced oxygen diffusion along the grain boundaries. This assumption implies that the grain boundary diffusion may be the dominant mechanism of mass transport during sintering, causing densification [7]. This may well be accepted in our case, since we are dealing with nanosized powder particles. In this case the fraction of the grain boundaries in the samples being sintered is extremely high. With introducing La^{3+} at A site the same situation as described above, as far as point defects are concerned appears. On the other hand in the case of co-doped sample some free ceria was detected as mentioned, and the influence of dopants on densification cannot be discussed on the basis of the results obtained [7].

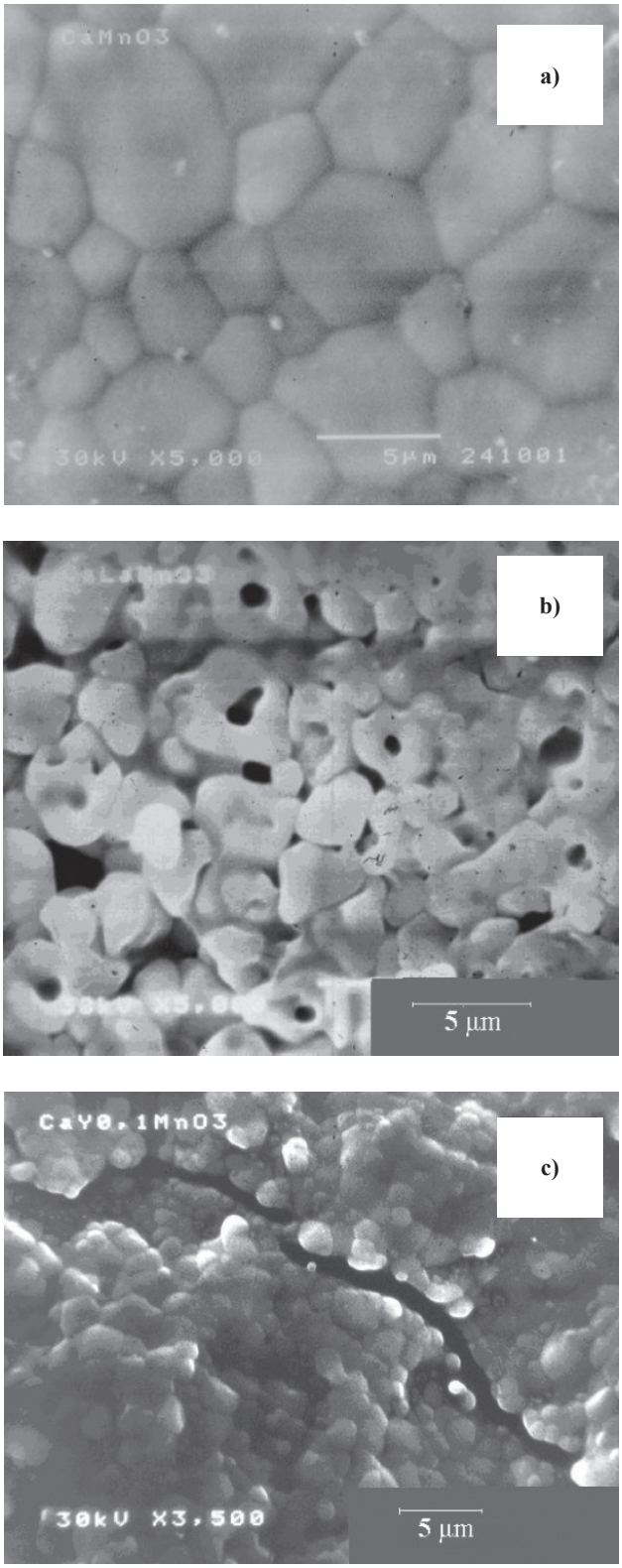

Figure 11. SEM micrographs of sintered pure and doped $CaMnO_3$; (a) pure $CaMnO_3$, (b) La doped $CaMnO_3$ and (c) Y doped $CaMnO_3$ sintered at optimum temperatures

SEM micrographs of sintered samples are presented in Fig. 11 [7]. It can be seen that the densities of undoped and Y doped samples achieved high degree, while in La doped samples considerable fraction of closed porosity can be observed. The pores are located both between and within the grains. In addition, it is obvious, that by doping $CaMnO_3$ grain growth process is largely affected. Both dopants, La and Y, suppress grain growth, which is especially outlined in Y containing samples. On the basis of these results it is obvious that Y cations promote densification, as well as, formation of fine grained microstructures, that is important for the properties, like electrical conductivity, given in Fig. 12.

The effect of doping and the electrical conductivity temperature behaviour of different $CaMnO_3$ based compositions can be seen in Fig. 12 [7]. The obtained results clearly show that both La and Y doped compositions, exhibit high electrical conductivity, both at room and high temperature, being in the range from $3.2 \cdot 10^2$ S/cm and $1.7 \cdot 10^2$ S/cm. Bearing in mind that for useful SOFC operation the acceptable levels of electrical conductivity for cathode material is $\sigma > 10^2$ S/cm [4], the electrical conductivity of the obtained perovskite solid solutions $Ca_{0.7}La_{0.3}MnO_3$, $Ca_{0.8}Y_{0.2}MnO_3$ and $Ca_{0.7}Y_{0.3}MnO_3$ satisfy this requirements.

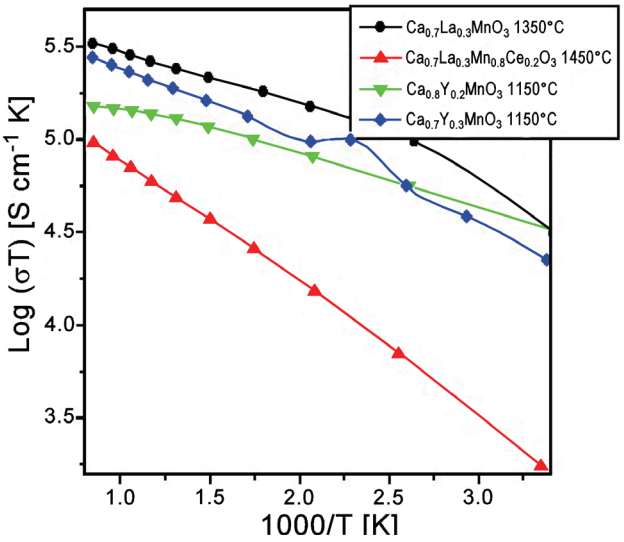

Figure 12. Plot Log (σT) vs. 1/T for doped $CaMnO_3$

IV. Conclusions

A short review of our recent results on the synthesis of nanosized CeO_2, $CaMnO_3$ and $BaCeO_3$ solid solutions is presented.

During self propagating room temperature synthesis (SPRT) the reaction proceeds via several intermediate stages due to the stepwise release of crystalline water from nitrate. The reaction steps, however, develop very fast and cannot be observed in the reacting mixture. On the basis of Raman spectroscopy studies it was shown that the solid solutions of $Ce_{1-x}Me_xO_{2-y}$ with one and two dopants can be synthesized by SPRT. It should be emphasized that:

- The reaction starting at room temperature is much less energy consuming in comparison with other methods of powder preparation;
- Single phase nanopowders are obtained in a very short time near the room temperature;
- Chemical composition can be controlled with a good precision;
- Calcination step is not needed;
- Simplicity of equipment is advantageous and cannot be neglected.

Glycine nitrate process (GNP) was modified (MGNP) by partial substitution of nitrates for acetates. The combustion process proceeded very smoothly. Powders with perovskite type structure with cation dopants on A as well as on B sites, or both, were synthesized. Loss of powder during synthesis was negligible. The amount of 100 g of powder was produced per run. Very precise stroichiometry was obtained in accordance with tailored composition. Powders were very active, clean, single phase and nanometric in size. It should be pointed out again, that by applying this method:

- Large amount of powder can be produced in a very short time;
- Single phase nanopowders with high specific surface area (among highest published**)** area are obtained;
- No intermediate phases were detected;
- Instrumentation is very simple;
- Very precise control of stoichimetry is possible all over the batch;
- The method is flexible of forming complex compositions.

Sintering test for manganites showed that full density was achieved at lower sintering temperatures. Increasing Y concentration enhanced densification of manganites, and suppressed grain growth process during sintering. Electrical conductivity is highly accepted for SOFC components.

Acknowledgement: The authors are grateful to Ministry of Education and Science of the Republic of Serbia, The Humboldt Foundation, Germany, and National Science and Engineering Council of Canada, for supporting this paper which is a part of III 45012 project.

References

1. X. Yu, F. Li, X. Ye, X. Xin, Z. Xue, "Synthesis of cerium (IV) oxide ultrafine particles by solid-state reactions", *J. Am. Ceram. Soc*., **83** [4] (2000) 964–966.
2. L.A. Chick, L.R. Pederson, G.D. Maupin, J.L. Bates, L.E. Thomas, G.J. Exarhos, "Glycine-nitrate combustion synthesis of oxide ceramic powders", *Mater. Lett.*, **10** [1-2] (1990) 6–12.
3. S. Bošković, D. Djurović, Z. Dohčević-Mitrović, Z. Popović, M. Zinkevich, F. Aldinger, "Self-propagating room temperature synthesis of nanopowders for solid oxide fuel cells (SOFC)", *J. Power Sources*, **145** [2] (2005) 237–242.
4. S.B. Bošković, B.Z. Matović, M.D. Vlajić, V.D. Krstić, "Modified glycine nitrate procedure (MGNP) for the synthesis of SOFC nanopowders", *Ceram. Int.*, **33** [1] (2007) 89–93.
5. S. Boskovic, S. Zec, M. Ninic, J. Dukic, B. Matovic, D. Djurovic, F. Aldinger, "Nanosized Ceria Solid Solutions Obtained by Different Chemical Routs", *J. Optoelectron. Adv. Mater.*, **10** [3] (2008) 515–519.
6. Z.D. Dohčević-Mitrović, M.J. Šćepanović, M.U. Grujić-Brojčin, Z.V. Popović, S.B. Bošković, B.M. Matović, M.V. Zinkevich, F. Aldinger ,"The size and strain effects on the Raman spectra of $Ce_{1-x}Nd_xO_{2-\delta}$ ($0 \le x \le 0.25$) nanopowders", *Solid State Commun.*, **137** [7] (2006) 387–390.
7. Z.D. Dohčević-Mitrović, M. Sćepanović, M. Grujić-Brojčin, Z.V. Popović, S. Bošković, B. Matović, M. Zinkevich, F. Aldinger, "$Ce_{1-x}Y(Nd)_xO_{2-\delta}$ nanopowders: potential materials for intermediate temperature solid oxide fuel cells", *J. Phys.- Condens. Mater.*,**18** [33] (2006), S2061–S2068.
8. B. Matović, J. Dukić, A. Devečerski, S. Bošković, M. Ninić, Z. Dohčević-Mitrović, "Crystal structure analysis of Nd-doped ceria solid solutions", *Sci. Sintering,* **40** (2008) 63–68.
9. S. Bošković, J. Dukić, B. Matović, Lj. Živković, M. Vlajić, V. Krstić, "Synthesis, sintering and electrical conductivity of calcium manganite solid solutions", *J. Alloy. Compd*., **463** [1-2] (2008) 282–287.
10. J. Dukić, S. Bošković, B. Matović, B. Dimčić, Lj. Karanović, "Ritweld refinement of crystal phases $(Ca_{1-x}La_x)MnO_3$ with perovskite-type structure", *Mater. Sci. Forum*, **518** (2007) 233F.
11. R.D. Shannon, "Revised effective ionic radii and systematic studies of interatomic distances in halides and chalkogenides", *Acta Crystallogr.*, **A32** (1976) 751–767
12. A. Kroeger, *Point Defects in Compounds and Their Role in Diffusion, Sintering and Related Phenomena*, Ed. C.G. Kuczynski, Gordon and Breatch Science Publ. 1967.